Reflectance and transmittance model for recto-verso halftone prints: spectral predictions with multi-ink halftones

Mathieu Hébert* and Roger David Hersch

Ecole Polytechnique Fédérale de Lausanne (EPFL), School of Computer and Communication Sciences, 1015 Lausanne, Switzerland
**Corresponding author: mathieu.hebert@epfl.ch*

Received October 30, 2008; accepted December 9, 2008;
posted December 15, 2008 (Doc. ID 103419); published January 28, 2009

We extend a previously proposed spectral reflectance and transmittance prediction model for recto-verso prints to the case of multi-ink halftones. The model takes into account the multiple reflections and the lateral propagation of light within the paper substrate (optical dot gain) as well as the spreading of the inks according to their superposition conditions (mechanical dot gain). The model accounts for the orientation of the incident and exiting lights when traversing the halftone ink layers, which enables modeling the measuring geometry. The equations for the calibration of the model and for the predictions are presented in detail. Several experiments with inkjet prints show that the multi-ink halftone transmittance model is as accurate as the actually most performing reflectance models for halftone prints.

OCIS codes: 100.2810, 120.5700, 120.7000.

1. INTRODUCTION

Thanks to the recent advances in the modeling of the reflection of light by halftone prints, it is now possible to predict printed colors with a very good accuracy. The best predictions are obtained with spectral models that account for the lateral propagation of light into the paper substrate (optical dot gain) and the spreading of the inks (physical dot gain) according to their superposition with the other inks [1]. However, none of the existing models enables predicting the color of the prints when they are seen in transmittance mode. In a recent work [2], we proposed a first spectral reflectance and transmittance model for recto-verso halftone prints, where each side of the paper may be printed with a different colorant. We now propose to extend this model in order to account for any type of multi-ink recto-verso halftone print.

The reflectance and transmittance prediction model is based on a description of the multiple reflections of light between the paper substrate and the print-air interfaces. It was inspired by the well-known Clapper–Yule model [3] and also influenced by Williams and Clapper [4] by taking into account the orientation of light within the colorant layers. In contrast with these reflectance-only models, where the paper is simply considered as a reflecting background, the reflectance and transmittance model includes the transmission of light through the paper. This yields a multiple reflection process between the top print-air interface, the paper layer, and the bottom print-air interface. The multiple reflection process can be represented by an infinite graph [2] or by a Markov chain [5]. Simple formulas relying on seven parameters are obtained for the print reflectance and for the print transmittance. Three parameters characterize the paper substrate (top-side reflectance, bottom-side reflectance, and transmittance) and four parameters related to the interfaces and the inks express the attenuation of (1) the incident light, (2) the exiting light, (3) the light internally reflected by the top print-air interface, and (4) the light internally reflected by the bottom print-air interface. These four parameters are calculated according to Beer's law and to Fresnel's formulas as functions of the orientation of light, which enables taking into account the measuring geometry.

Such as for the reflectance-only prediction models, the reflectance and transmittance prediction model is calibrated by deducing from measurements the different parameters relative to the paper and to the inks: reflectance and transmittance of the paper, transmittance of the colorants, and correspondence between nominal-to-effective surface coverage of the different inks [1]. To cope with the most general printing configuration, we present the calibration procedure by considering that the recto and the verso are printed with different inks. This procedure may obviously be simplified when the two sides are identical and printed with the same sets of inks under the same conditions.

This paper is structured as follows: first, we describe the recto-verso print and present the reflection and transmission model (Section 2). The terms specific to the attenuation of light by the inks and the interfaces are developed in Section 3. Then, in Section 4, we explain the calibration procedure and expand the prediction formulas in Section 5. Finally, we propose an experimental validation of the model in Section 6. The conclusions are drawn in Section 7.

2. RECTO-VERSO PRINT

A recto-verso print is a sheet of paper or of diffusing plastic whose two faces are printed with halftone colors. We

call "recto" the side seen by the observer or the detector. Thus, the light source illuminates the recto in reflectance mode and the verso in transmittance mode.

The unprinted paper sheet is assumed to be symmetric, i.e., the same reflectance can be measured on its two faces. The paper substrate is absorbing and strongly scattering. Its refractive index, generally close to 1.5, is denoted as n_p. Considered without its bounding interfaces, the substrate layer has an intrinsic reflectance $\rho(\lambda)$ and an intrinsic transmittance $\tau(\lambda)$ assumed independent of the angular distribution of light.

Halftone colors are obtained by printing two, three, or four inks according to dot screens that partially overlap each other. In the overlap areas, the superposed inks form new colorants. For example, a yellow ink superposed with a magenta ink yields a red colorant. A halftone of N inks is a mosaic of 2^N colorants. Each colorant is characterized by its surface coverage a_k on the paper and its normal transmittance t_k, which describes the attenuation of directional light crossing it perpendicularly. At an oblique incidence angle θ, the light follows a path of length $1/\cos\theta$. It is therefore attenuated, according to Beer's law [6], by a factor of $t^{1/\cos\theta}$.

The mosaic of colorants forms a single "inked layer," that has the same refractive index n_p as the paper. Its normal transmittance is given by Neugebauer's equation

$$t = \sum_{k=1}^{2^N} a_k t_k. \tag{1}$$

For oblique incident light, the attenuation is

$$\sum_{k=1}^{2^N} a_k t_k^{1/\cos\theta}. \tag{2}$$

Since the inked layer forms the interface between the print and the air, we aggregate the attenuation by the inked layer and the reflectivity and transmittivity of the interface. The inked layer aggregated to the interface is called a "colored interface."

Thanks to the concept of the colored interface, every print is modeled by three superposed elements: the substrate layer at the center, a recto colored interface, and a verso colored interface. When a face of the paper is not printed, the corresponding colored interface is simply the air-paper interface. Between these three elements, light undergoes multiple reflections and transmissions [2,7,8]. The reflectance of the print, measured on the recto side by discarding the surface reflection component (gloss), is expressed as

$$R = T_{\text{in}} T_{\text{ex}} \frac{\rho - r_2(\rho^2 - \tau^2)}{(1 - r_1\rho)(1 - r_2\rho) - r_1 r_2 \tau^2}, \tag{3}$$

where r_1 is the internal reflectance of the recto colored interface, r_2 is the internal reflectance of the verso colored interface, T_{in} is a "penetration term" characterizing the transmission of the incident light through the recto colored interface, and T_{ex} is an "exit term" characterizing the transmission of the emerging light through the recto colored interface.

The transmittance of the print, illuminated at the verso side and observed at the recto side, is expressed as

$$T = T_{\text{in}} T_{\text{ex}} \frac{\tau}{(1 - r_1\rho)(1 - r_2\rho) - r_1 r_2 \tau^2}, \tag{4}$$

where r_1, r_2, and T_{ex} have the same meaning as in Eq. (3) and where the penetration term T_{in} characterizes the transmission of the incident light through the verso colored interface.

Thanks to the generic terms T_{in}, T_{ex}, r_1, and r_2, Eqs. (3) and (4) stand for any recto-verso print. However, these terms are expressed differently according to the printed inks and the measuring geometry. Section 3 gives a survey of their different possible expressions.

3. REFLECTANCE AND TRANSMITTANCE OF THE COLORED INTERFACES

A colored interface comprises the print–air interface and possibly an inked layer. To express its reflectance and transmittance, we first recall how the light is reflected and transmitted by the paper-air interface alone. Then, we add a uniform colorant layer or a mosaic of colorants. In each case, we first develop reflectance and transmittance expressions for directional light, then for diffuse light. We finally present the expressions for r_1, r_2, T_{in}, and T_{ex} corresponding to these different types of colored interfaces and to typical measuring geometries.

A. Air–Print Interfaces

The paper has a refractive index, n_p, different from the one of air that is close to 1. Hence, the print–air interface reflects and transmits light according to Snell's laws and Fresnel's formulas [9]. Let us denote air and paper using the respective subscripts 0 and 1. The air-face of the interface, illuminated at angle θ_0, has a reflectivity denoted as $R_{01}(\theta_0)$ and a transmittivity denoted as $T_{01}(\theta_0)$. Since the energy is conserved at the interface, we have

$$R_{01}(\theta_0) + T_{01}(\theta_0) = 1. \tag{5}$$

The paper-face of the interface, illuminated at angle θ_1, has a reflectivity denoted as $R_{10}(\theta_1)$ and a transmittivity denoted as $T_{10}(\theta_1)$. Once again, we have

$$R_{10}(\theta_1) + T_{10}(\theta_1) = 1. \tag{6}$$

For θ_0 and θ_1 related according to Snell's law, i.e., $\theta_1 = \arcsin(\sin\theta_0/n_p)$, we also have

$$T_{01}(\theta_0) = T_{10}(\theta_1), \tag{7}$$

$$R_{01}(\theta_0) = R_{10}(\theta_1). \tag{8}$$

When the interface is illuminated by Lambertian light, its reflectance and its transmittance integrate the reflectivity, respectively, the transmittivity, of each incident light ray. They are therefore expressed by integrals, presented in detail in [2]. The air-face reflectance is expressed as

$$r_{01} = \int_{\theta_0=0}^{\pi/2} R_{01}(\theta_0)\sin 2\theta_0 \mathrm{d}\theta_0, \tag{9}$$

the paper-face reflectance as

$$r_{10} = \int_{\theta_1=0}^{\pi/2} R_{10}(\theta_1)\sin 2\theta_1 \mathrm{d}\theta_1, \tag{10}$$

the air-to-paper transmittance as

$$t_{01} = \int_{\theta_0=0}^{\pi/2} T_{01}(\theta_0)\sin 2\theta_0 \mathrm{d}\theta_0 = 1 - r_{01}, \tag{11}$$

and the paper-to-air transmittance as

$$t_{10} = \int_{\theta_1=0}^{\pi/2} T_{10}(\theta_1)\sin 2\theta_1 \mathrm{d}\theta_1 = 1 - r_{10}. \tag{12}$$

B. Colored Interface Comprising a Solid Colorant Layer

Consider the paper printed with a solid colorant layer having the same refractive index n_p as the paper. The junction of this interface and of the colorant layer forms a colored interface whose reflectance and transmittance for directional light are given in Fig. 1.

When the incident light is Lambertian, the reflectance and the transmittance integrates the reflectance, respectively, the transmittance, of each incident ray. They are therefore expressed by integrals similar to those presented in the case of the interface alone. At the air-side, since the light does not reach the inked layer, the diffuse reflectance of the colored interface is r_{01} expressed by Eq. (9). At the paper-side, the light rays cross twice the colorant layer. The diffuse reflectance is

$$r_{10}(t) = \int_{\theta_1=0}^{\pi/2} R_{10}(\theta_1)t^{2/\cos\theta_1}\sin 2\theta_1 \mathrm{d}\theta_1. \tag{13}$$

Similarly, the air-to-paper transmittance is given by

$$t_{01}(t) = \int_{\theta_0=0}^{\pi/2} T_{01}(\theta_0)t^{1/\cos\theta_1}\sin 2\theta_0 \mathrm{d}\theta_0, \tag{14}$$

and the paper-to-air transmittance by

$$t_{10}(t) = \int_{\theta_1=0}^{\pi/2} T_{10}(\theta_1)t^{1/\cos\theta_1}\sin 2\theta_1 \mathrm{d}\theta_1. \tag{15}$$

These integrals may be cumbersome to calculate. Instead, we recommend using the following functions that provide excellent approximations:

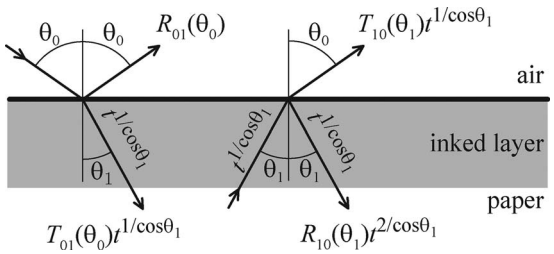

Fig. 1. Reflection and transmission of directional light at the air-side and paper-side of a colored interface.

$$r_{10}(t) \simeq r_{10}\frac{e^{t^\beta} - 1}{e - 1}, \tag{16}$$

$$t_{01}(t) \approx t_{01}t^\mu, \tag{17}$$

$$t_{10}(t) \approx t_{10}t^\mu, \tag{18}$$

where β and μ are constants that depend only on the refractive index n_p. For $n_p = 1.5$, we have $\beta = 2.945$ and $\mu = 1.13$. The values of $r_{10}(t)$ as a function of t are tabulated in [2].

C. Colored Interface Comprising a Halftone Inked Layer

When the paper is printed with an N-ink halftone, the inked layer is composed of a mosaic of 2^N colorants, where each colorant k is characterized by its surface coverage a_k and its normal transmittance t_k. The reflectance (respectively, the transmittance) of the colored interface is the sum of the reflectances (respectively, the transmittances) of the individual colorants weighted by their respective surface coverage. The directional air-to-print transmittance is given by

$$T_{01}(\theta_i)\sum_{k=1}^{2^N} a_k t_k^{1/\cos\theta_i'}, \tag{19}$$

where θ_i is the angle of incidence and $\theta_i' = \arcsin(\sin\theta_i/n_p)$ is the angle at which the light is refracted into the inked layer. For a Lambertian illumination, according to Eq. (14) and to approximation (17), the diffuse air-to-paper transmittance of the colored interface is given by

$$t_{01}(a_k,t_k) = \sum_k a_k t_{01}(t_k) \simeq t_{01}\sum_k a_k t_k^\mu. \tag{20}$$

Likewise, the diffuse paper-to-air transmittance is given by

$$t_{10}(a_k,t_k) = \sum_k a_k t_{10}(t_k) \simeq t_{10}\sum_k a_k t_k^\mu. \tag{21}$$

The paper-side diffuse reflectance $r_{10}(a_1,a_2,\ldots,a_8,t_1,t_2,\ldots,t_8)$, denoted as $r_{10}(a_k,t_k)$ for short, is

$$r_{10}(a_k,t_k) = \sum_k a_k r_{10}(t_k). \tag{22}$$

D. Expressions for r_1, r_2, T_{in} and T_{ex}

Let us now establish the expressions for the parameters r_1, r_2, T_{in}, and T_{ex} used in Eqs. (3) and (4). Reflectances r_1 and r_2 represent the diffuse reflectance of the recto, respectively, the verso, colored interfaces. For the unprinted paper, they are equal to the diffuse reflectance r_{10} of the print-air interface alone, therefore given by Eq. (10). When the paper is printed, they are given by Eq. (13) when the inked layer is a solid colorant layer or by Eq. (22) when the inked layer is a halftone. Note that the typical refractive index of prints $n_p = 1.5$ yields a diffuse reflectance r_{10} close to 0.6. This means that 60% of the light diffused by the substrate is internally reflected and therefore that an important amount of light is subject to multiple reflections within the print.

The penetration term T_{in} describes the transmission of the incident light through the colored interface at the illuminated side. It is an air-to-paper transmittance that therefore depends on the incident angular distribution. Its expression is given in Table 1 for directional or diffuse incident light and for colored interfaces comprising no ink, a solid colorant layer, or a halftone inked layer.

The exit term T_{ex} describes the attenuation of the light transiting from the paper to the capturing device (e.g., radiance detector or integrating sphere). It is a paper-to-air transmittance and depends on the capture geometry. In the case of a radiance detector, according to [10], T_{ex} comprises the transmittivity of the interface, multiplied by the oblique transmittance of the inked layer and by a factor $1/n_p^2$ characteristic of cone spreading due to the refraction at the interface [11]. In the case of an integrating sphere, T_{ex} is simply the diffuse paper-to-air transmittance of the colored interface. The different expressions for T_{ex} are given in Table 2.

E. Orientational and Nonorientational Models

The reflectance and transmittance model accounts for the orientation of light when calculating its attenuation by the inks. This makes sense when the colorants are nonscattering and do not penetrate much into the paper. Otherwise, scattering breaks the directionality of light and the colorant transmittance can be assumed independent of the angular distribution. Clapper and Yule [3] already noted this phenomenon and ignored the orientation of light in their "nonorientational" model. Mathematically, as shown in [10] in the case of the Clapper–Yule and Williams–Clapper models, an orientational model is converted into its nonorientational version by removing every exponent on the colorant transmittance. In the present reflectance and transmittance model, this yields only two modifications: setting $\mu=1$, where μ is the constant introduced in Eq. (17), and replacing the diffuse reflectance given by Eq. (13) with the following one:

$$r_{10}(t) = r_{10}t^2. \tag{23}$$

Table 1. Expressions for T_{in}

Inked Layer	Directional Light Source[a]	Lambertian Light Source
No ink	$T_{01}(\theta_i)$	t_{01}
Solid colorant	$T_{01}(\theta_i)t^{1/\cos\theta_i'}$	$t_{01}(t)\approx t_{01}t^{\mu}$
Halftone	$T_{01}(\theta_i)\Sigma_k a_k t_k^{1/\cos\theta_i'}$	$t_{01}(a_k,t_k)\approx t_{01}\Sigma_k a_k t_k^{\mu}$

[a]Where θ_i is the angle of incidence and $\theta_i'=\arcsin(\sin\theta_i/n_p)$ is the angle at which the light is refracted into the inked layer.

Table 2. Expressions for T_{ex}

Inked Layer	Radiance Detector[a]	Integrating Sphere
No ink	$T_{10}(\theta_x')n_p^{-2}$	t_{10}
Solid colorant	$T_{10}(\theta_x')n_p^{-2}t^{1/\cos\theta_x'}$	$t_{10}(t)\approx t_{10}t^{\mu}$
Halftone	$T_{10}(\theta_x')n_p^{-2}\Sigma_k a_k t_k^{1/\cos\theta_x'}$	$t_{10}(a_k,t_k)\approx t_{10}\Sigma_k a_k t_k^{\mu}$

[a]The angle of observation being θ_x, $\theta_x'=\arcsin(\sin\theta_x/n_p)$ is the angle followed by the captured light before being refracted at the print–air interface. Note that $T_{01}(\theta_x)=T_{10}(\theta_x')$ according to Eq. (7).

4. CALIBRATION OF THE TRANSMITTANCE MODEL

The calibration step consists of deducing from measurements all the parameters used in the spectral prediction model, except the print's refractive index n_p, which is assumed to be known. We first determine the parameters relative to the paper, i.e., the substrate layer intrinsic reflectance $\rho(\lambda)$ and intrinsic transmittance $\tau(\lambda)$; then the parameters relative to the recto and the verso colorants, i.e., their normal transmittances $t_1(\lambda),t_2(\lambda),\ldots,t_1'(\lambda),t_2'(\lambda),\ldots$ and their respective surface coverages $a_1,a_2,\ldots,a_1',a_2',\ldots$.

The calibration procedure relies on a certain set of printed patches that are measured and for which we develop the reflectance expression, or accordingly the transmittance expression, in respect to the geometry used for the measurement. It would be tedious to duplicate here the equations for all the possible measuring geometries. Therefore, we consider only the de:0° geometry, where a radiance detector is located at 0° in front of the recto and where a diffuse light source illuminates either the recto side in reflectance mode (gloss excluded) or the verso side in transmittance mode.

A. Paper Parameters

The intrinsic reflectance $\rho(\lambda)$ and transmittance $\tau(\lambda)$ of the paper substrate layer are deduced from reflectance and transmittance measurements of the paper sheet. The paper reflectance $R(\lambda)$ is expressed by Eq. (3) with r_1 and r_2 given by Eq. (10), T_{in} given by the top right formula in Table 1 and T_{ex} given by the top left formula in Table 2. We obtain

$$R = t_{01}T_{10}(0)n_p^{-2}\frac{\rho - r_{10}(\rho^2-\tau^2)}{(1-r_{10}\rho)^2 - r_{10}^2\tau^2}. \tag{24}$$

The paper transmittance $T(\lambda)$ is expressed by Eq. (4), with the same expressions as above for r_1, r_2, T_{in}, and T_{ex}. We obtain

$$T = \frac{t_{01}T_{10}(0)n_p^{-2}\tau}{(1-r_{10}\rho)^2 - r_{10}^2\tau^2}. \tag{25}$$

From Eqs. (24) and (25), using the notations

$$R' = \frac{R}{t_{01}T_{10}(0)n_p^{-2}}$$

$$T' = \frac{T}{t_{01}T_{10}(0)n_p^{-2}},$$

we deduce the two following equations, valid for each wavelength of the light:

$$\rho = \frac{R' + r_{10}(R'^2 - T'^2)}{(1+r_{10}R')^2 - r_{10}^2T'^2}, \tag{26}$$

$$\tau = \frac{T'}{(1 + r_{10}R')^2 - r_{10}^2 T'^2}. \quad (27)$$

When $n_p = 1.5$, we have $T_{10}(0) = 0.96$, $r_{10} = 0.60$, and $t_{01} = 0.91$ [12].

B. Colorant Normal Transmittances

To determine the normal transmittance spectrum $t_u(\lambda)$ of a recto colorant, we print a solid layer of this colorant on the recto side and measure the transmittance $T(\lambda)$ of this print. The measured transmittance is expressed by Eq. (4) with $r_1 = r_{10}(t_u)$, $r_2 = r_{10}$, $T_{\text{in}} = t_{01}$ (first row, right column of Table 1) and $T_{\text{ex}} = t_u T_{10}(0) n_p^{-2}$ (second row, left column of Table 2). We obtain

$$T = \frac{t_u t_{01} T_{10}(0) n_p^{-2} \tau}{[1 - r_{10}(t_u)\rho][1 - r_{10}\rho] - r_{10}(t_u) r_{10} \tau^2}. \quad (28)$$

In Eq. (28), all the terms are known except t_u, which can be computed by solving numerically Eq. (28) wavelength by wavelength. When the recto is printed with N inks, this procedure is repeated for the 2^N colorants.

A similar procedure is followed to determine the normal transmittance t'_u of the verso colorants. Since the ink is now in front of the light source, the expression for the measured transmittance is slightly different. The penetration term is $T_{\text{in}} = t_{01} t'^{\mu}_u$ (second row, right column of Table 1 and the exit term is $T_{\text{ex}} = T_{10}(0) n_p^{-2}$ (first row, left column of Table 2). The recto and verso diffuse reflectances are, respectively, $r_1 = r_{10}$ and $r_2 = r_{10}(t'_u)$. The measured print transmittance is expressed by

$$T = \frac{t'^{\mu}_u t_{01} T_{10}(0) n_p^{-2} \tau}{[1 - r_{10}\rho][1 - r_{10}(t'_u)\rho] - r_{10} r_{10}(t'_u) \tau^2}. \quad (29)$$

Thus, t'_u is obtained by solving numerically Eq. (29) for each wavelength. When the verso is printed with N' inks, this procedure is repeated for the $2^{N'}$ colorants.

Note that Eqs. (28) and (29) are very close to each other. They differ only by an exponent μ applied to the ink normal transmittance at the numerator. This difference is due to the fact that the incident light and the captured light have different angular distributions, being, respectively, Lambertian and directional. When the inks are nonscattering and do not penetrate into the paper, this distinction is crucial to ensure the accuracy of the model.

C. Effective Surface Coverages

At printing time, the ink dots generally spread out to an extent that depends on the printing device and the type of paper. Due to this "dot gain" phenomenon, the surface coverage of each ink is different from the one initially expected. It was also shown that the inks spread differently when they are alone on paper or superposed with other inks [1,13]. Hence, we print a single ink halftone at 50% nominal surface coverage either on paper alone or superposed with solid layers of the other inks.

Let us call t_v the transmittance of the solid colorant layer v (which may be the paper alone), t_{u+v} the transmittance of the dots of ink u printed on solid colorant v, and $a_{u/v}$ their effective surface coverage. The transmittance of the printed patch is expressed by Eq. (4) with $T_{\text{in}} = t_{01}$ and $r_2 = r_{10}$ since there is no ink on the verso and with

$$r_1 = a_{u/v} r_{10}(t_{u+v}) + (1 - a_{u/v}) r_{10}(t_v), \quad (30)$$

$$T_{\text{ex}} = [a_{u/v} t_{u+v} + (1 - a_{u/v}) t_v] T_{10}(0) n_p^{-2}. \quad (31)$$

The transmittance of the printed patch is therefore

$$T = \frac{[a_{u/v} t_{u+v} + (1 - a_{u/v}) t_v] t_{01} T_{10}(0) n_p^{-2} \tau}{(1 - r_1\rho)(1 - r_{10}\rho) - r_1 r_{10} \tau^2} \quad (32)$$

with r_1 given by Eq. (30).

The single unknown parameter in Eq. (32) is $a_{u/v}$. It is computed numerically as the value that minimizes the sum of the squared differences between the measured values $\tilde{T}(\lambda)$ and the values predicted according to formula (32)

$$a_{u/v} = \min_{0 \le a \le 1} \sum_{\lambda=380\text{ nm}}^{730\text{ nm}} \left\{ \tilde{T} - \frac{t_{01} T_{10}(0) n_p^{-2} \tilde{\tau} [a \tilde{t}_{u+v} + (1 - a) \tilde{t}_v]}{(1 - r_{10}\tilde{\rho})(1 - \tilde{r}_1\tilde{\rho}) - r_{10}\tilde{r}_1\tilde{\tau}^2} \right\}^2, \quad (33)$$

where symbol $\sim$ indicates the wavelength-dependent terms and $\tilde{r}_1 = a r_{10}(\tilde{t}_{u+v}) + (1-a) r_{10}(\tilde{t}_v)$.

It is assumed that the effective surface coverage is 0, respectively, 1, when the nominal surface is 0% (no ink), respectively, 100% (full coverage). We have therefore the effective surface coverage for the three following nominal surface coverages: 0%, 50%, and 100%. By interpolating these values linearly, we obtain a curve that gives for any nominal surface coverage the corresponding effective surface coverage. An example of this curve, called the "nominal-to-effective surface coverage function" $f_{u/v}(a)$, is shown in Fig. 2. Note that in order to obtain a smoother nominal-to-effective surface coverage function, we can calculate additional effective surface coverage values by printing the inks at, for example, 25%, 50%, and 75% nominal surface coverage.

This procedure is repeated for each ink and for each configuration of superposition with another colorant. For example, with cyan, magenta, and yellow inks, we follow the procedure for cyan halftones printed on paper white, on magenta solid layer, on yellow solid layer, and on red solid layer, for magenta halftones (alone, on solid cyan ink, on solid yellow ink, and on solid green colorant) and for yellow halftones (alone, on solid cyan ink, on solid ma-

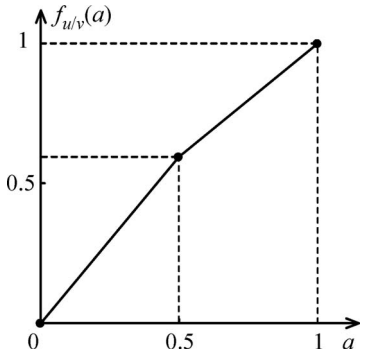

Fig. 2. Nominal-to-effective surface coverage function representing the effective surface coverage of a halftone ink as a function of the nominal surface coverage a.

genta ink, and on solid blue colorant). The procedure is then repeated at the verso by using Eq. (4) with the following terms:

$$T_{\text{in}} = t_{10}[(1 - a'_{u/v})t'^{\mu}_{u+v} + a'_{u/v}t'^{\mu}_{v}],$$

$$T_{\text{ex}} = T_{10}(0)n_p^{-2},$$

$$r_1 = r_{10},$$

$$r_2 = a'_{u/v}r_{10}(t'_{u+v}) + (1 - a'_{u/v})r_{10}(t'_v).$$

D. List of Calibration Patches and of the Computed Parameters

For a complete calibration in the case of three-ink halftones, 20 different patches are needed at the recto side; the eight solid colorant patches are used to deduce the colorant transmittances (including the paper white) and the 12 patches permitting to deduce the nominal-to-effective surface coverage functions, where each ink is printed at 50% while the two other inks are printed at 0% or 100%. The same number of patches are needed at the verso side. Note that only eight calibration patches are needed in the case of two-ink halftones.

During the calibration process, the following parameters are computed (for cyan, magenta, and yellow halftones): substrate intrinsic reflectance $\rho(\lambda)$ and transmittance $\tau(\lambda)$; the normal transmittances of the recto colorants cyan $t_c(\lambda)$, magenta $t_m(\lambda)$, yellow $t_y(\lambda)$, red $t_{m+y}(\lambda)$, green $t_{c+y}(\lambda)$, blue $t_{c+m}(\lambda)$, and black $t_{c+m+y}(\lambda)$; the normal transmittance of the verso colorants cyan $t'_c(\lambda)$, magenta $t'_m(\lambda)$, yellow $t'_y(\lambda)$, red $t'_{m+y}(\lambda)$, green $t'_{c+y}(\lambda)$, blue $t'_{c+m}(\lambda)$, and black $t'_{c+m+y}(\lambda)$; the nominal-to-effective surface coverage functions for the ink halftones on the recto, i.e., f_c for cyan alone, $f_{c/m}$ for cyan superposed with magenta, $f_{c/y}$ for cyan superposed with yellow, $f_{c/m+y}$ for cyan superposed with both magenta and yellow, f_m for magenta alone, $f_{m/c}$ for magenta superposed with cyan, $f_{m/y}$ for magenta superposed with yellow, and $f_{m/c+y}$ for magenta superposed with both cyan and yellow, f_y for yellow alone, $f_{y/c}$ for yellow superposed with cyan, $f_{y/m}$ for yellow superposed with magenta, and $f_{y/c+m}$ for yellow superposed with both cyan and magenta. In addition, the nominal-to-effective surface coverage functions for the ink halftones on the verso also need to be computed (same list as for the recto).

5. SPECTRAL PREDICTIONS

Once all the calibration steps have been performed, we can start making reflectance and transmittance predictions for various surface coverages of the recto-verso prints. Let us consider a three-ink recto-verso halftone print with given nominal surface coverages on the recto and on the verso. The first prediction step consists of computing the effective surface coverage of each colorant. Then, the transmittance spectrum is predicted thanks to Eq. (4). Such as in the Section 4, the reflectance and transmittance measurements rely on the de:0° geometry, where a Lambertian light source illuminates the recto in reflectance mode, or the verso in transmittance mode, and a radiance detector is located at 0° in front of the recto.

A. Effective Surface Coverages

On the recto, the three inks (cyan, magenta, and yellow) are printed with the respective nominal surface coverages c_0, m_0, and y_0. The corresponding effective surface coverages c, m, and y, accounting for the spreading of each ink in the different superposition conditions, are obtained by performing several iterations of the following equations, taking $c=c_0$, $m=m_0$, and $y=y_0$ as initial values [1]:

$$\begin{aligned} c &= (1-m)(1-y)f_c(c_0) + m(1-y)f_{c/m}(c_0) \\ &\quad + (1-m)yf_{c/y}(c_0) + myf_{c/m+y}(c_0), \\ m &= (1-c)(1-y)f_m(m_0) + c(1-y)f_{m/c}(m_0) \\ &\quad + (1-c)yf_{m/y}(m_0) + cyf_{m/c+y}(m_0), \\ y &= (1-c)(1-m)f_y(y_0) + c(1-m)f_{y/c}(y_0) \\ &\quad + (1-c)mf_{y/m}(y_0) + cmf_{y/c+m}(y_0). \end{aligned} \tag{34}$$

The effective surface coverage of the colorants white (a_w), cyan (a_c), magenta (a_m), yellow (a_y), red (a_{m+y}), green (a_{c+y}), blue (a_{c+m}), and black (a_{c+m+y}), are obtained using Demichel's equations [14]:

$$\begin{aligned} a_w &= (1-c)(1-m)(1-y), \\ a_c &= c(1-m)(1-y), \\ a_m &= (1-c)m(1-y), \\ a_y &= (1-c)(1-m)y, \\ a_{m+y} &= (1-c)my, \\ a_{c+y} &= c(1-m)y, \\ a_{c+m} &= cm(1-y), \\ a_{c+m+y} &= cmy. \end{aligned} \tag{35}$$

The same procedure is followed for the verso colorants, where the cyan, magenta, and yellow inks are printed with nominal surface coverages c'_0, m'_0, and y'_0. We obtain the effective surface coverages a'_k for the eight colorants.

B. Transmittance Predictions

The transmittance spectrum $T(\lambda)$ of the recto-verso print is predicted thanks to Eq. (4) with T_{in}, T_{ex}, r_1, and r_2 expressed as

$$T_{\text{in}} = t_{01}\sum_k a'_k t'^{\mu}_k, \quad T_{\text{ex}} = T_{10}(0)n_p^{-2}\sum_k a_k t_k, \tag{36}$$

$$r_1 = \sum_k a_k r_{10}(t_k), \quad \text{and } r_2 = \sum_k a'_k r_{10}(t'_k),$$

where $r_{10}(t)$ is calculated according to Eq. (13) or according to its approximation (16).

For each wavelength, the transmittance of the recto-verso halftone print is given by

$$T = \frac{t_{01}T_{10}(0)n_p^{-2}\tau(\Sigma a'_k t'^{\mu}_k)(\Sigma a_k t_k)}{[1-\rho\Sigma a_k r_{10}(t_k)][1-\rho\Sigma a'_k r_{10}(t'_k)]-[\Sigma a_k r_{10}(t_k)][\Sigma a'_k r_{10}(t'_k)]\tau^2}. \quad (37)$$

C. Reflectance Predictions

The reflectance of the recto-verso print is expressed by Eq. (3) with T_{ex}, r_1 and r_2 expressed as in Eq. (36), and T_{in} expressed as in Eq. (36) but relative to the recto colorants

$$T_{in} = t_{01}\sum_k a_k t_k^{\mu}. \quad (38)$$

The print reflectance is therefore given by

$$R = \frac{t_{01}T_{10}(0)n_p^{-2}(\Sigma a_k t_k^{\mu})(\Sigma a_k t_k)[\rho-(\rho^2-\tau^2)\Sigma a'_k r_{10}(t'_k)]}{[1-\rho\Sigma a_k r_{10}(t_k)][1-\rho\Sigma a'_k r_{10}(t'_k)]-[\Sigma a_k r_{10}(t_k)][\Sigma a'_k r_{10}(t'_k)]\tau^2}. \quad (39)$$

Our experience shows that if the ink normal transmittances and the nominal-to-effective surface coverage curves are calibrated from transmittance measurements, formula (39) may give inaccurate predictions. Diffusion of light within the colorants is probably at the origin of this lack of accuracy. Instead, we recommend performing a second calibration from reflectance measurements.

The calibration procedure in reflectance mode is exactly the same as in transmittance mode by using Eq. (3) in place of Eq. (4) with T_{in} being relative to the recto colorants instead of the verso colorants. Note, however, that the influence of the verso colorant decreases strongly as the paper opacity increases. For very opaque papers, the verso colorants can be simply assimilated to the background reflectance. Thus, as shown in [2], the recto-verso reflectance model becomes equivalent to a Williams–Clapper model extended to halftones

$$R = \frac{t_{01}T_{10}(0)n_p^{-2}(\Sigma a_k t_k^{\mu})(\Sigma a_k t_k)\rho_B}{1-\rho_B\Sigma a_k r_{10}(t_k)}, \quad (40)$$

where $\rho_B(\lambda)$ is the reflectance of the paper background.

6. EXPERIMENTAL VERIFICATION

To verify the prediction model, we printed recto-verso halftone patches with the Canon PixmaPro 9500 inkjet printer. A first set of 1875 patches was printed with cyan, magenta, and yellow inks at 120 lines per inch (lpi) on the super-calendered and nonfluorescent paper APCO II from Scheufelen Company, Germany. Then, a second set of 41 patches was printed at different screen frequencies and on different types of papers with cyan, magenta, and yellow inks on the recto and red and green custom inks on the verso. The reflectance and transmittance measurements were performed using the Color i7 instrument from X-rite Company.

The color differences between measured and predicted spectra are expressed in CIELAB ΔE_{94} values. They are obtained by converting the predicted and measured spectra into CIE-XYZ tristimulus values, calculated with a D65 illuminant, and in respect to a 2° standard observer. The CIE-XYZ values are then converted into CIELAB color coordinates using as a white reference the unprinted paper color obtained by reflectance spectrum (in reflectance mode), respectively, the transmittance spectrum (in transmittance mode), of the paper illuminated with the D65 illuminant [16].

A. Verification with 1875 CMY Recto-Verso Patches

A set of 1875 patches was printed on the APCO paper at 120 lpi with cyan, magenta, and yellow inks. On the recto, we printed the 125 combinations of the three inks at 0%, 25%, 50%, 75%, and 100%. On the verso, we printed the 15 colors listed in Table 3. The ΔE_{94} values presented in Table 3 correspond to the average CIELAB ΔE_{94} difference between the measured and predicted transmittance spectra, calculated for each different verso color over the 125 recto colors, as well as the ΔE_{94} 95-quantile. The very low ΔE_{94} differences between measurements and predictions shows the excellent accuracy of the transmittance model when calibrated in transmittance mode.

Table 3. Average Color Difference between Measured and Predicted Transmission Spectra

Verso	Average ΔE_{94}[a]	95-Quantile
Unprinted	0.71	1.57
Solid cyan	1.22	2.21
Solid magenta	0.90	1.92
Solid yellow	0.75	1.60
Solid red	1.04	1.80
Solid green	1.37	2.33
Solid blue	0.97	1.81
Solid black	1.33	2.20
50% cyan	1.03	2.10
50% magenta	0.89	1.79
50% yellow	1.02	1.95
50% red	1.13	1.97
50% green	1.03	1.78
50% blue	1.17	2.12
50% black	1.06	2.10
Total average	**1.04**	**2.09**

[a]Average over the 125 different recto patches.

The reflectance prediction model was tested on the 125 patches whose verso was unprinted. The model was calibrated from reflectance measurements. We obtained an average CIELAB ΔE_{94} of 0.70 and a 95-quantile of 1.45. These values are very close to those obtained in transmittance for the same color patches. We thus conclude that the reflectance model and the transmittance model have the same accuracy. As expected, we obtained exactly the same prediction results by using the Williams–Clapper model extended to multi-ink halftones, expressed by Eq. (40).

By way of comparison, we also tested the nonorientational version of the reflectance and transmittance model. As explained in Section 3, the nonorientational model is obtained simply by setting exponent μ to 1 and replacing the expression for $r_{10}(t)$ by Eq. (23). The calibration and the predictions are performed with these new equations. The prediction results are almost identical to the ones obtained with the orientational models; in transmittance mode, we obtained an average ΔE_{94} of 1.01 over the 1875 recto-verso patches with a 95-quantile of 2.02; in reflectance mode, we obtained an average ΔE_{94} of 0.72 over the 125 recto-only patches with a 95-quantile of 1.56. As we can see, the orientational model is not really more accurate than the nonorientational model for the prints considered in this experiment. We explain this by the fact that a part of the inks penetrates the paper and therefore scatters a small portion of the light.

B. Influence of the Paper and of the Halftone Screen Frequency

In a second experiment, we tested the transmittance model with recto-verso prints produced by using different inks on the recto and the verso. The recto was printed with cyan (C), magenta (M), and yellow (Y) inks and the verso was printed with red (R) and green (G) custom inks. In addition to the 19 recto-only patches and the seven verso-only patches required to calibrate the model, we printed 41 verification patches. The recto and verso layouts were generated at different halftone screen frequencies: 60, 90, 120, and 150 (lpi). They were printed on the super-calendered nonfluorescent APCO II paper. The layout generated at 120 lpi was also printed on common office paper and on nonfluorescent Biotop paper. The color differences between measures and predictions, averaged over the 41 recto-verso patches, are presented in Table 4. We can see that the transmittance model provides excellent predictions independently of the screen frequency.

Table 4. Average Color Difference between Measured and Predicted Transmission Spectra

Type of Paper	Halftone Screen Frequency (lpi)	Average ΔE_{94}[a]	95-Quantile
APCO II paper	60	0.92	1.81
	90	0.81	1.56
	120	0.99	1.56
	150	0.87	1.45
Office paper	120	0.63	1.17
Biotop paper	120	1.17	2.11

[a]Average over the 41 different recto-verso patches.

Predictions are slightly less accurate with Biotop paper because the inks penetrate deeply into the paper and become diffusing, whereas they are assumed rather transparent in our model [2]. The best prediction accuracy is obtained with office paper on which the inks are deposited more homogeneously.

7. CONCLUSIONS

The previously developed reflectance and transmittance model for recto-verso halftone prints [2] was extended to multi-ink halftones with the possibility to print different inks on the recto and on the verso. The model accounts for the specific enlargement of the ink dots when superposed with the dots of other inks (ink spreading) as well as for the specific attenuation of light according to its orientation and according to the measuring geometry. It relies on a reduced number of parameters and requires a small set of recto-only and verso-only patches for calibration. On each side, twenty patches are needed for three-ink halftones or eight patches for two-ink halftones. Various experiments performed with inkjet prints proved that the transmittance model reaches the accuracy level of the best reflectance prediction models with an average CIELAB ΔE_{94} difference between measured and predicted transmittance spectra close to 1 for a set of 1875 CMY recto-verso halftone patches, printed over 60 distinct sheets. Furthermore, the prediction accuracy seems to be independent of the halftone screen frequency and to be weakly affected by the penetration of the inks into certain types of paper. In the future, it would be interesting to test the model when its underlying assumptions of strong scattering by the paper and of low scattering by the inks are not verified, i.e., with more opaque inks and more translucent paper.

REFERENCES

1. R. D. Hersch, P. Emmel, F. Collaud, and F. Crété, "Spectral reflection and dot surface prediction models for color halftone prints," J. Electron. Imaging **14**, 33001–33012 (2005).
2. M. Hébert and R. D. Hersch, "A reflectance and transmittance model for recto-verso halftone prints," J. Opt. Soc. Am. A **22**, 1952–1967 (2006).
3. F. R. Clapper and J. A. C. Yule, "The effect of multiple internal reflections on the densities of halftone prints on paper," J. Opt. Soc. Am. **43**, 600–603 (1953).
4. F. C. Williams and F. R. Clapper, "Multiple internal reflections in photographic color prints," J. Opt. Soc. Am. **29**, 595–599 (1953).
5. M. Hébert, R. D. Hersch, and J.-M. Becker, "Compositional reflectance and transmittance model for multilayer specimens," J. Opt. Soc. Am. A **24**, 2628–2644 (2007).
6. H.-H. Perkampus, *Encyclopedia of Spectroscopy* (VCH, 1995).
7. J. W. Ryde, "The scattering of light by turbid media," Proc. R. Soc. London, Ser. A **131**, 451–475 (1931).
8. G. Kortüm, "Phenomenological theories of absorption and scattering of tightly packed particles," in *Reflectance Spectroscopy* (Springer Verlag, 1969), Chap. 4, pp. 103–168.
9. M. Born and E. Wolf, *Principle of Optics*, 7th ed. (Pergamon, 1999), p. 40.
10. M. Hébert and R. D. Hersch, "Classical print reflection models: a radiometric approach," J. Imaging Sci. Technol. **48**, 363–374 (2004).

11. W. R. McCluney, *Introduction to Radiometry and Photometry* (Artech, 1994), pp. 7–13.
12. D. B. Judd, "Fresnel reflection of diffusely incident light," J. Res. Natl. Bur. Stand. **29**, 329–332 (1942).
13. P. Emmel and R. D. Hersch, "Modeling ink spreading for color prediction," J. Imaging Sci. Technol. **46**, 237–246 (2002).
14. M. E. Demichel, Procédé **26**, 17–21 (1924), see also [15].
15. D. R. Wyble and R. S. Berns, "A critical review of spectral models applied to binary color printing," Color Res. Appl. **25**, 4–19 (2000).
16. G. Sharma, "Color fundamentals for digital imaging," in *Digital Color Imaging Handbook*, G. Sharma, ed. (CRC, 2003), pp. 30–36.